Eight Years of Science with Chandra / Chandra Calibration Workshop 2007: #124

Status of the HRC−I QE and QEU

J. Posson−Brown, V. Kashyap (CXC/SAO)

Quantum Efficiency

- HRC-I quantum efficiency (QE) is monitored with regular observations of standard candles including HZ 43, G21.5-0.9, and Cas A.
- Aimpoint QE is constant over time at low energies (see Figure 1) and high energies (see Figures 2 and 3).
- The absolute calibration of the QE matches the HRC-S and ACIS-I within spectral model uncertainties (see Figures 1-3).

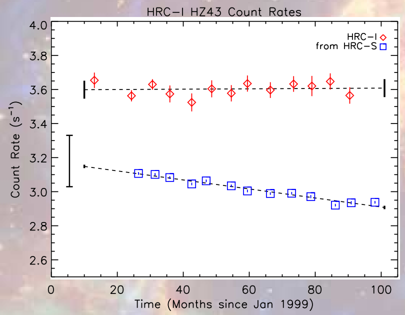

Figure 1: Background-subtracted 0^{th} order count rates from HRC HZ 43 calibration observations taken regularly since launch. The red diamonds show HRC-I aimpoint count rates, and the blue squares show HRC-S aimpoint count rates transformed to the HRC-I QE. (That is, the HRC-S count rates have been divided by 2.67, since a rate of 1 ct/s on the HRC-I equals 2.67 ct/s on the HRC-S for HZ 43, assuming a blackbody model with kT = 4 eV and nH = $1{\times}10^{17}$ cm^{-2}.) The small error bars on the points show the statistical error. The black dashed lines are linear fits to the points, with vertical bars bracketing the lines giving the error on the best-fit slopes. The large vertical bar on the left shows the magnitude of uncertainty on the HRC-S to HRC-I conversion factor. Note that the HRC-I slope is consistent with zero, while the HRC-S slope indicates a QE drop with time.

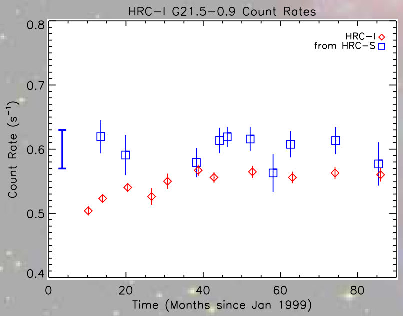

Figure 2: Background-subtracted count rates from HRC G21.5-0.9 calibration observations taken regularly since launch. The red diamonds show HRC-I count rates, and the blue squares show HRC-S count rates transformed to the HRC-I QE. (That is, the HRC-S count rates have been divided by 0.82, since a rate of 1 ct/s on the HRC-I equals 0.82 ct/s on the HRC-S for G21.5-0.9, assuming a powerlaw model with Γ = 1.9 and nH = $2.1{\times}10^{22}$ cm^{-2}.) The small error bars on the points show the statistical errors. The large blue vertical bar on the left shows the magnitude of uncertainty on the HRC-S to HRC-I conversion factor.

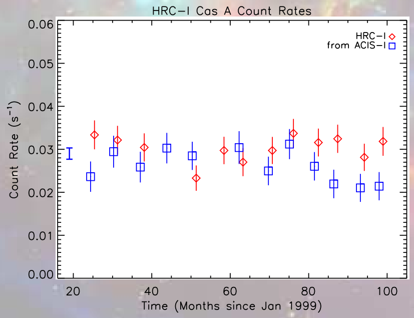

Figure 3: Background-subtracted count rates from HRC-I and ACIS-I calibration observations of Cas A taken regularly since launch. These count rates are for the central point source in Cas A. The red diamonds show HRC-I count rates, and the blue squares show ACIS-I count rates transformed to the HRC-I QE with a time-dependent conversion factor (to account for changes to the ACIS-I QE since launch), assuming a powerlaw model with Γ = 3.13 and nH = $1.68{\times}10^{22}$ cm^{-2} (Chakrabarty et al, 2001 ApJ, 548, 800). The small error bars on the points show the statistical errors. The blue vertical bar on the left shows the magnitude of uncertainty on the ACIS-I to HRC-I conversion factor.

QE Uniformity

- Capella observations at 40 locations on the detector indicate that QEU map is good to $<$ 2% at high energies (see Figure 4).
- Multiple RXJ 1856 observations indicate that the low energy QE is depressed at Z=+10′; the Capella observation at this location indicates that this depression is not seen at higher energies (see Figure 5). (Similarly, repeated HZ 43 observations at Y=+10′ show a low-energy QE depression, while observations of Vela indicate that the depression at this location is not seen at higher energies. See “Studying the HRC-I Uniformity with Observations of the Vela SNR”, Posson-Brown & Donnelly, 2004 Chandra Calibration Workshop.)
- HZ 43 observations at Y=+10′ and RXJ 1856 observations at Z=+10′ also indicate that the QE at these locations is dropping with time (see Figure 6). The rate of decline seen with HZ 43 at Y=+10′ is similar to that seen on the HRC-S with HZ 43; the rate of decline at Z=+10′ seen with RXJ 1856 is steeper.

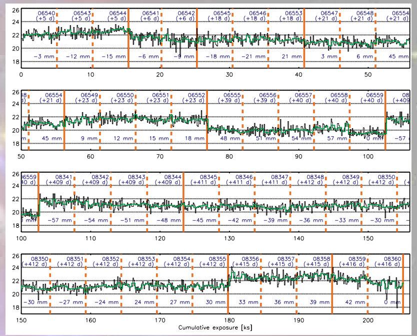

Figure 4: The combined light curve of all HRC-I observations of Capella, spanning 205 ks. The black histogram denotes the count rate for a binning of 100 s, and overlaid on it is the count rate for a binning of 500 s (green histogram). The data gaps between observations are excluded, and indicated by vertical red lines (solid when the gaps are $>$ 100 s, dashed otherwise). The data comprise 40 ObsIDs (noted at the top of each segment, along with the day since 2005-dec-01 that the observation started). The SIM offset at which each observation is carried out is indicated at the bottom of each segment. The counts are corrected by the QE uniformity at each observation location. Note that the count rate is fairly constant over sequential observations, despite the changes in position on the detector. By calculating the change in count rate between sequential observations, we see that the current QEU map is accurate to $\sim$ 1.6% at these observation locations. (Figure from Eight Years of Science with Chandra poster #55, Kashyap & Posson-Brown.)

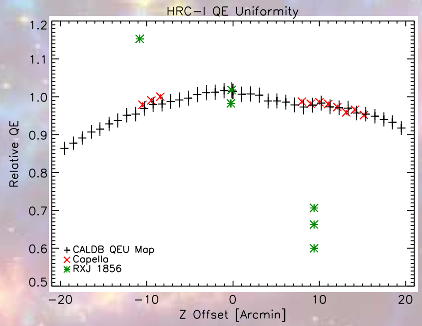

Figure 5: HRC-I quantum efficiency relative to the detector aimpoint at the locations of the forty Capella observations (see Figure 4). The black crosses show the values from the CALDB QEU map, with error bars showing 2% uncertainty. The red Xs show QEU factors derived from Capella count rates from 11 sequential observations (ObsIDs 8345 - 8355) where the source count rate is assumed constant. (That is, the red Xs show the count rates for these observations relative to the average count rate of the aimpoint observations.) The green asterisks show QEU factors derived from aimpoint and offset RXJ 1856 observations. While factors derived from Capella match very well with the CALDB map, the factors from RXJ 1856 suggest that the map is inaccurate at low energies. In particular, the low energy QE appears depressed at Z=+10′.

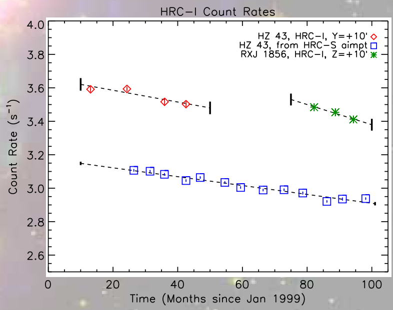

Figure 6: The HRC-I QE declines at Y=+10’, shown by HZ 43 (red diamonds) and at Z=+10’, shown by RXJ 1856 (green asterisks). For display purposes, the HZ 43 points have been offset by +0.6 and the RXJ 1856 points by +3.0. The black dashed lines show linear fits to the points, with vertical bars bracketing the lines showing the error on the best-fit slopes. The blue squares show the HZ 43 count rates on the HRC-S transformed to the HRC-I QE, as in Figure 1. The rates of QE decline seen by the HZ 43 observations at the HRC-S aimpoint and HRC-I Y=+10’ are similar, but the rate of decline shown by RXJ 1856 at Z=+10’ is steeper.

Supported by NASA contract NAS8−39073

Cas A image from http://chandra.harvard.edu